PROCEEDINGS A

rspa.royalsocietypublishing.org

Perspective

Cite this article: Phillips D. 2016 A lifetime in photochemistry; some ultrafast measurements on singlet states. *Proc. R. Soc. A* **472**: 20160102.
http://dx.doi.org/10.1098/rspa.2016.0102

Received: 11 February 2016
Accepted: 29 April 2016

Subject Areas:
photochemistry

Keywords:
photochemistry, singlet states, ultrafast measurements

Author for correspondence:
David Phillips
e-mail: d.phillips@imperial.ac.uk

A lifetime in photochemistry; some ultrafast measurements on singlet states

David Phillips

Department of Chemistry, Imperial College London, Exhibition Road, London SW7 2AZ, UK

We describe here the development of time-correlated single-photon counting techniques from the early use of spark discharge lamps as light sources through to the use of femtosecond mode-locked lasers through the personal work of the author. We used laser-excited fluorescence in studies on energy migration and rotational relaxation in synthetic polymer solutions, in biological probe molecules and in supersonic jet expansions. Time-correlated single-photon counting was the first method used in early fluorescence lifetime imaging microscopy (FLIM), and we outline the development of this powerful technique, with a comparison of techniques including wide-field microscopy. We employed these modern forms of FLIM to study single biological cells, and applied FLIM also to gain an understanding the distribution in tissue, and fates of photosensitizer molecules used in photodynamic therapy. We also describe the uses and instrumental design of laser systems for the study of ultrafast time-resolved vibrational spectroscopy.

1. Introduction

Photochemistry, the study of the physical and chemical fates of polyatomic molecules excited electronically by the absorption of ultraviolet, visible and in some cases, near-infrared light was until the 1960s a phenomenological subject only, because absolute rates of decay of the electronically excited states of molecules first reached upon absorption, almost invariably a singlet state, were nanosecond to subnanosecond, then too short to measure easily.

The excitation and decay processes are conveniently summarized in the so-called Jablonski diagram (figure 1) [1]. The ground electronic state of most polyatomic molecules is a singlet state, with the highest occupied molecular orbital accommodating two electrons with

THE ROYAL SOCIETY PUBLISHING

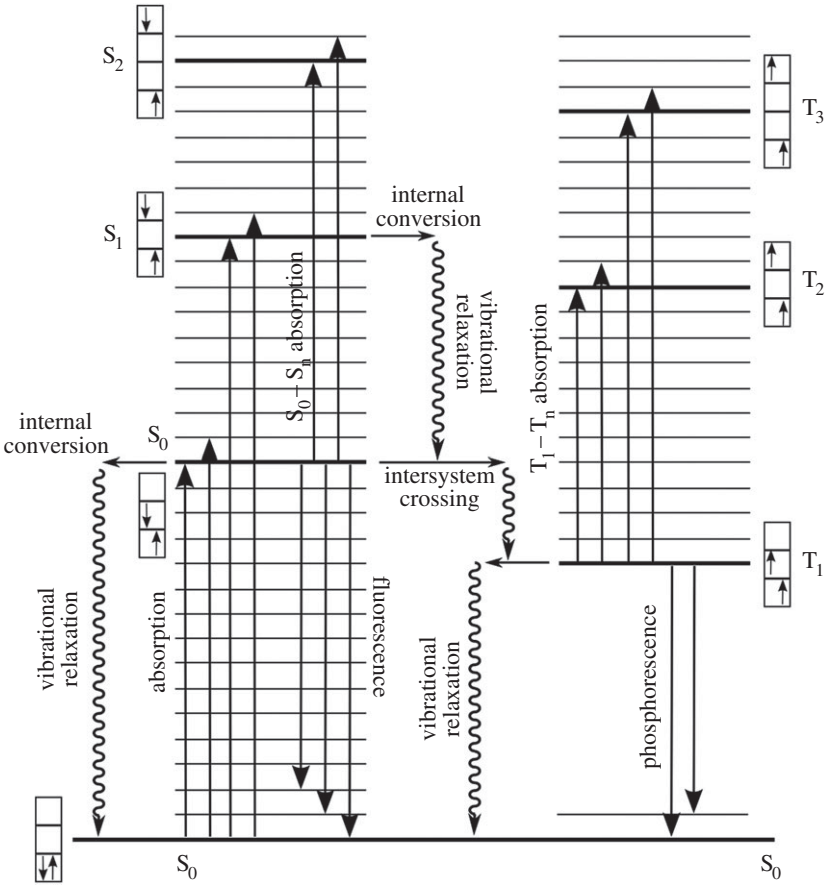

Figure 1. Jablonski representation of the fates of excited states of polyatomic molecules. [1] S denotes singlet (spin paired) states, T denotes triplet states with unpaired spins, thus paramagnetic states. In most molecules, very fast relaxation to the S_1 and T_1 states precedes observable photophysics and chemistry. Solid lines represent radiative processes, wavy lines non-radiative. The occupancy of molecular orbitals and spin of electrons is indicated in the boxes. (Adapted from [1].)

opposed spins. Upon excitation by absorption of light, the spin state is unchanged in an electric dipole allowed transition, thus producing an electronically excited singlet state, which can decay by spontaneous emission (*fluorescence*), or can undergo a spin inversion process, *intersystem crossing*, producing the electronically excited triplet state, which is invariably longer lived than the singlet state. Other non-radiative decay processes (*internal conversion*) compete with the radiative, and *chemistry* can also occur from any electronically excited state; *quenching*, with other ground-state molecules (*chemistry*, *complex formation* including *exciplexes* and *excimers*, *charge transfer*, *electron transfer* and *energy transfer* processes) complete the picture.

Writing a simple kinetic scheme permits definition of the quantum yield of any process, typified by fluorescence, ϕ_F and fluorescence decay time τ_F in terms of first-order rate constants for the processes depicted in figure 1, where k_{NR} is the sum of the rate constants for all first-order non-radiative processes depleting the excited state population, k_{ISC}, k_{IC}, k_D, etc.

$$^1M^* \rightarrow M + h\nu \quad k_R \text{ (fluorescence)} \tag{1.1}$$

$$^1M^* \rightarrow {}^3M^* \quad k_{ISC} \text{ (intersystem crossing)} \tag{1.2}$$

$$^1M^* \rightarrow M \quad k_{IC} \text{ (internal conversion)} \tag{1.3}$$

and

$$^1M^* \rightarrow \text{products} \quad k_D \text{ (dissociation)} \tag{1.4}$$

From a steady-state analysis of the scheme, the quantum yield of fluorescence ϕ_F is given by

$$\phi_F = \frac{k_R}{(k_R + k_{ISC} + k_{IC} + k_D)} \tag{1.5}$$

The fluorescence lifetime or commonly decay time, τ_F is the time a fluorophore remains in its excited state after excitation, and can vary from a few nanoseconds to subpicosecond.

$$\tau_F = (k_R + k_{ISC} + k_{IC} + k_D)^{-1} \tag{1.6}$$

The natural or radiative lifetime τ_0 is that which the molecule would have if emission were the only decay process.

$$\tau_0 = k_R^{-1} = \frac{\tau_F}{\phi_F}. \tag{1.7}$$

If there is quenching by another molecule present, Q, then, in addition to the terms in the denominator, there will appear the term $k_Q\,[Q]$, where k_Q is the quenching rate constant, and $[Q]$ is the quencher concentration.

Fluorescence also exhibits polarization effects, measured by the intensity components of fluorescence which are polarized parallel to the plane of polarization of excitation radiation, I_{II}, and that perpendicular, $I_\perp$. The Perrin equation relates anisotropy r to the initial anisotropy, r_0, the fluorescence decay time τ_F, and the rotational relaxation time of the fluorophore, τ_r (equations (1.8) and (1.9)). The relevant equations for the time-dependence of the components are given in equations (1.10) to (1.16). The time-dependent anisotropy is a measure of the ease with which the fluorophore can rotationally relax in the medium in which the fluorophore is placed, and can be used to measure the viscosity of the medium.

$$\frac{1}{r} = \frac{1}{r_0}\left[1 + \frac{3\tau_F}{\tau_r}\right] \tag{1.8}$$

$$r = \frac{(I_{II} - I_\perp)}{(I_{II} + 2I_\perp)} \tag{1.9}$$

$$I_{II}(t) = e^{-t/\tau_F}(1 + 2r_0 e^{-t/\tau_r}) \tag{1.10}$$

$$I_\perp(t) = e^{-t/\tau_F}(1 - r_0 e^{-t/\tau_r}) \tag{1.11}$$

$$F(t) = I_{II}(t) + 2I_\perp(t) \tag{1.12}$$

$$= 3e^{-t/\tau_F} \tag{1.13}$$

$$= F_0 e^{-t/\tau_F} \tag{1.14}$$

$$r(t) = \frac{I_{II}(t) - I_\perp(t)}{I_{II}(t) + 2I_\perp(t)} \tag{1.15}$$

$$= r_0 e^{-t/\tau_r} \tag{1.16}$$

Referring back to figure 1, until the 1960s, relative yields of fluorescence, intersystem crossing and some chemistry could be determined, but in the absence of absolute rates of decay, further progress in rationalizing photochemistry could not be made. Attempts were made to estimate these rate constants by use of the *Strickler–Berg* equation (see below). All changed with the advent of the technique of time-correlated single-photon counting (TCSPC) and the complementary, sometimes competitive approach of frequency-domain fluorescence decay methods. The author has been involved in the development and utilization of TCSPC techniques over the duration of his scientific life, and offers this personal perspective on their evolution, with some case histories from his own and others' work.

2. Time-correlated single-photon counting

Before the advent of mode-locked lasers, conventional discharge lamps could be produced which had very low intensities, but short decay times in the ns region. When used to excite

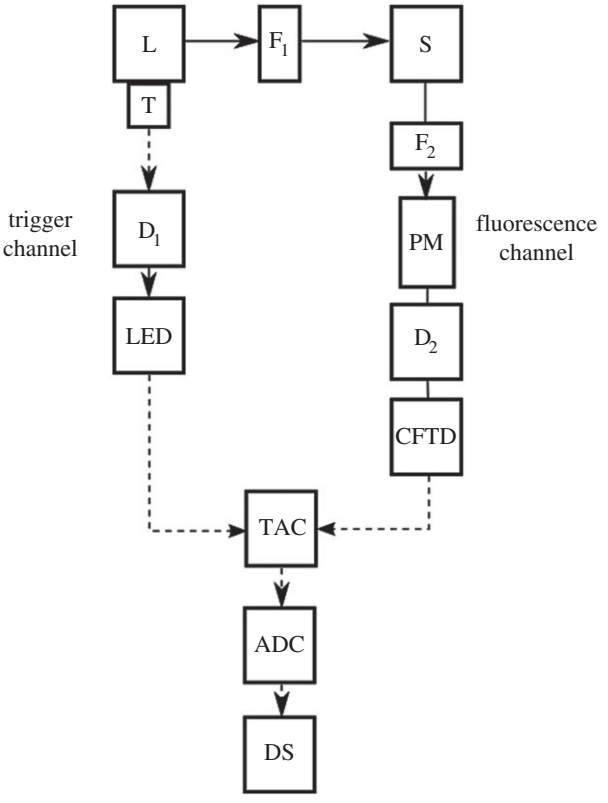

Figure 2. Time-correlated single-photon counting methodology [1]. Block diagram of an early conventional single photon counting apparatus. Solid line, optical signal, dotted line electronic signal. L is the excitation source (lamp or laser); T the trigger, (antenna, fibre optic and photomultiplier, etc.); S is sample holder; F_1, F_2 filter or monochromator; PM a fast photomultiplier tube or microchannel plate; D_1, D_2 delay lines; LED a leading edge timing discriminator; CFTD, a constant fraction timing discriminator; TAC, a time-to-amplitude converter; ADC, an analogue-to-digital converter; DS, a data store (multichannel analyser or computer). Adapted from [1].

molecules, ensuing fluorescence could then be detected using the extremely sensitive technique of time-correlated single-photon counting [1,2]. The technique is illustrated in figure 2.

Excitation of the sample by a light pulse initiates a linearly rising voltage ramp in a time-to-amplitude converter, the process being stopped by the detection of an emitted fluorescence photon. One count is then stored in a bin, and the process repeated, thus building up a histogram of probability of emission as a function of time, which, with a sufficient number of counts, resolves into a smooth decay curve that can then be analysed. Extraction of decay data and modelling of decay parameters are usually performed using a method of iterative convolution of excitation lamp and instrument response functions with trial decays until a good fit is obtained [1,2]. Models might include multiple exponentials, $t^{-1/2}$ terms and others [1–3], though great care is needed in attaching physical significance to the fitting parameters extracted.

In principle, decay parameters can be obtained reliably which are around one-tenth of the instrument response function, typically 2 ns for a discharge lamp excitation. However, spark discharge lamps suffered from great variability in intensity and profile, and highly variable time between pulses, making them difficult to use. It was the advent of mode-locked lasers in the 1970s, with very short, intense pulses of light and highly reproducible pulse profiles and time between pulses which led to a huge increase in the reliability of the TCSPC technique [4–9], and to developments such as time-resolved fluorescence spectroscopy [10], and fluorescence lifetime imaging microscopy (FLIM; see below). The most recent stable instrument response function

from an ultrafast TCSPC experimental set-up has been given as 17.8 ps (W. Becker, 2016, private communication), implying that fluorescence decays as short as approximately 1–2 ps can now be measured with great accuracy by TCSPC. Standards for comparison of results from different techniques are essential, and we have contributed to a number of these being established over three decades [11–13].

We were among the first to use mode-locked lasers for TCSPC studies, in vinyl aromatic synthetic polymer solutions [14–19] including studies on time-resolved fluorescence anisotropy [18]. The goal of this work was to achieve an understanding of the mechanism by which electronic energy migrated along the aromatic species pendant to the polymer chains, where rotational motion of the aromatic species had been invoked as a dominant mechanism, bringing the aromatic molecules into orientations such that energy transfer was facilitated; segmental motion of the polymer backbone had been deemed of importance, and the heterogeneity of the polymer samples also played a role, because aromatic molecules were randomly distributed along copolymer chains. After much effort over two decades, we came to the conclusion that modelling fluorescence decays obtained by mode-locked laser excitation and single-photon counting detection, while providing excellent results in terms of fitting to experimental decays, were unable definitively to distinguish between the various physical models upon which mathematical modelling was based. Some success was experienced, however, in observing polymers adsorbed on surfaces, using the technique of evanescent wave time-resolved fluorescence [20–22].

Early studies also investigated biological fluorescent probe molecules in simple systems such as model membranes, and the basic photophysics of the probes and models for the probes themselves. This was necessary because it was found that probes such as *dansyl* [23], and *indoles* [24,25] (which were models for *tryptophan* amino acid upon which many studies on proteins had been based), exhibited intrinsic complex decay functions, meaning that care had to be exercised in interpretation of fluorescence decay parameters in terms of biological phenomena alone [23–29]. Such complexities in fluorescence decays were also observed in molecules used as fluorescence standards, e.g. *quinine bisulfate* [29].

We also investigated the fluorescence decay of a molecule considered to be the prototypical species exhibiting intramolecular charge transfer (ICT), leading to dual fluorescence, *dimethylaminobenzonitrile*, (DMABN) [30]. Some very early time-resolved fluorescence studies were carried out on this and related molecules in ultra-cold supersonic jet expansions. In jet expansions, molecules are prepared with a very narrow velocity distribution, which effectively 'cools' the molecule to very low vibrational and rotational population distributions greatly simplifying spectra. For the first time, to the best of our knowledge, decay dynamics for single vibrational levels of the bare molecule, plus solvated complexes were obtained [31–33].

Time-correlated single-photon counting using cavity-dumped or pulse-picked selection of pulses quickly established itself as the workhorse for observing singlet state decay processes, and is almost universally employed in research laboratories worldwide for this purpose. The dynamic range is astonishing, (hundreds of nanoseconds to 1 ps), the accuracy unrivalled. Early applications of the technique included adding time-resolution to fluorescence microscopy, which had burgeoned with the development of confocal imaging, giving much sharper images capable of resolution in three dimensions. It had been proposed that where multiple fluorophores were excited, the added dimension of time-resolution could distinguish between them, yielding much enhanced biological information [34,35] (see also below; section Photodynamic therapy (PDT)).

3. Fluorescence lifetime imaging microscopy

The advances in the instrumentation associated with TCSPC have led to the widespread use of the technique in microscopy. Optical imaging techniques, in particular fluorescence imaging techniques, are powerful tools in the biological and biomedical sciences today, because they are minimally invasive and can be applied to live cells and tissues. Conventionally, microscopy

relies on the contrast that can be achieved from absorption, polarization, phase and fluorescence parameters in a fluorescence microscope. Conventionally, fluorescence intensity is measured, and three-dimensional images can be recorded using confocal (one or two-photon excitation, TPE) techniques. However, fluorescence intensity is dependent upon a variety of environmental influences, such as quenching by other molecules, aggregation, energy transfer and refractive index effects, and can thus be difficult to quantify or interpret.

FLIM provides contrast according to the fluorescence decay time, the inverse of the sum of the rate parameters for all depopulation processes (equation (1.6)). While the fluorescence decay time depends on the intrinsic characteristics of the fluorophore itself, it also depends in a measurable way upon the local environment in general, the local viscosity, pH or refractive index [36,37] as well as interactions with other molecules. Thus, as well as being able to distinguish spectrally similar fluorophores, imaging of the fluorescence lifetime can be used to probe the surroundings of a fluorophore [38,39]. In the last decade or so, since the first reports on FLIM the technique have been improved, developed further and applied to an increasing number of studies in cell biology.

To amplify the characteristics of FLIM, we can say it is a time-resolved image acquisition method, the technologies for which can be divided into two categories: (i) confocal scanning or multiphoton excitation FLIM where the image is acquired pixel-by-pixel using a non-imaging detector, e.g. a photomultiplier and (ii) wide-field camera-based FLIM [38,39]. The time-resolved information is obtained either in the time domain by exciting the sample with a short optical pulse and observing the decay of the fluorescence intensity (with TCSPC, gating or a streak camera), or in the frequency domain by modulating the excitation source and/or the detector to calculate the fluorescence decay time from the demodulation and the phase shift of the fluorescence.

In the time domain, a fluorescence decay curve can be directly acquired after excitation of the sample with an ultrashort light pulse, usually using a sampling technique. In wide-field time-gated FLIM, 'snapshots' of the fluorescence emission are taken at various nanosecond delays after the excitation using high-speed-gated image-intensified cameras [40]. This approach is fast, because all the pixels are acquired in parallel (a 100 Hz FLIM frame rate has been reported), but it lacks single photon sensitivity and accuracy, and its temporal resolution is limited to $\approx$80 ps (table 1).

In confocal scanning or multiphoton excitation microscopes (which provide inherent optical sectioning), FLIM is essentially a series of single channel fluorescence lifetime measurements where the fluorescence decay can be acquired by TCSPC. Here the ease of reproducibility of measurements is due to the unique combination of advantages such as the unlimited dynamic range associated with photon-counting techniques, linear recording characteristics independent of excitation intensity fluctuations and photo-bleaching, well-defined Poisson statistics, excellent signal-to-noise ratio and a high temporal (picosecond) resolution (table 1). However, as each photon is timed individually in each pixel of the image, the collection of many photons for a high statistical accuracy can be time-consuming [41]. The maximum photon flux that can be timed using a single channel one detector, time-to-amplitude converter and analogue to digital converter is limited by photon pile-up, and the dead time of the electronics to $\approx 10^6$ photons s^{-1}. A similar but rather faster approach is to bin all incoming photons within pre-set time windows after excitation. This time-binning method is significantly faster than TCSPC because it is not necessary to reduce the fluorescence signal to the level of single photon timing. However, it is less accurate than TCSPC (table 1).

The use of streak-camera-based FLIM has also recently been reported [42]. The technique works in line-scanning mode, is fast, has the highest temporal resolution of any FLIM technique, and it has been commercialized. In the frequency domain periodically modulated excitation beams and detectors may be used to measure the phase shift and demodulation of fluorescence signals with respect to their excitation signals, both in wide-field microscopy using modulated intensified cameras [43] and in confocal/multi-photon laser scanning microscopy using single channel detectors [44].

Table 1. Summary of some of the advantages and disadvantages of various implementations of FLIM (adapted from table 2 of ref. [38]).

implementation	advantages	disadvantages
time-gated wide-field time domain	fast	low sensitivity, need strong signal
	all pixels acquired in parallel	consecutive acquisition of time gates vulnerable to photo bleaching and sample movement
		poor spatial resolution due to phosphor screen on intensified CCD camera
		need pulsed laser
wide-field frequency domain	fast	cannot easily resolve two very different lifetimes
	easy to modulate continuous wave laser	vulnerable to photobleaching and sample movement
	can resolve two similar lifetimes	complex data and error analysis
	no deconvolution (temporal) of instrumental response and fluorescence decay necessary	
	all pixels acquired in parallel	poor spatial resolution due to phosphor screen on intensified CCD camera
		usually lower temporal resolution and Lower signal-to-noise ratio than time domain methods
confocal/multiphoton scanning with time-correlated single photon counting	single photon sensitivity	slow, each photon has to be timed individually
	unlimited dynamic range associated with photon counting techniques	need pulsed laser
	linear recording characteristics independent of excitation intensity fluctuations and photobleaching	
	easy visualization of fluorescence decays and well-defined Poisson statistics	
inherent optical sectioning	best signal-to-noise ratio	
	high temporal resolution	
confocal/multiphoton scanning with time-binning photon detection	fastest scanning technique	need pulsed laser
	inherent optical sectioning	slower than wide-field imaging
	single photon sensitivity	less accurate than time-correlated single photon counting
streak camera FLIM	very high temporal resolution	expensive
	fast	
	easy visualization of fluorescence decays	

Frequency domain techniques have been used since the 1920s to measure nanosecond fluorescence decays. With this approach, a fluorescence lifetime may be calculated from both the phase shift and demodulation (at several modulation frequencies if necessary). For a simple mono-exponential fluorescence decay profile, both calculations should yield the same value.

There is a lively debate as to the relative merits of time or frequency domain approaches to FLIM. In principle, they are, of course, related by a Fourier transformation and experimentally have been demonstrated to be equivalent. To non-specialists, the easy visualization of fluorescence decays in the time domain may be an advantage over the frequency domain, where the analysis of complex fluorescence decay profiles, such as stretched exponentials, is less tractable. However, for some applications, the frequency domain instrumentation is considered easier to implement, because ultrashort pulsed laser sources are not required, especially for longer lifetimes, although practitioners are increasingly using mode-locked lasers for frequency domain measurements frequency domain techniques are more photon efficient than time-gating techniques and require no deconvolution of the instrumental response and the fluorescence decay. The relative merits of the various FLIM implementations are summarized in table 1, and it depends on the operator's preference (and finances!) for fast data acquisition or accuracy, high temporal and spatial resolution which system to choose. These techniques complement the single-molecule fluorescence research recently honoured by the award of the 2015 Nobel Prizes for Chemistry to Moerner, Hell and Betzig.

4. Applications

Both TCSPC and wide-field approaches (figure 3) to fluorescence lifetime imaging microscopy on biological cells at Imperial College have yielded significant understanding of the biology. An emerging theme in cell biology is that cell surface receptors need to be considered as part of supramolecular complexes of proteins and lipids facilitating specific receptor conformations and distinct distributions, e.g. at the immunological synapse. There was a need to develop bioimaging that not only located proteins in live cells, but could also probe their environment, for example viscosity via rotational mobility through anisotropy measurements [45]. Such a technique was demonstrated using fluorescence lifetime imaging of green fluorescent protein (GFP) [46].

It was first shown by time-correlated single-photon counting, that the fluorescence decay of GFP depends on the local refractive index (figure 4). This dependence is not often explicitly considered in fluorescence studies, but is in agreement with the *Strickler–Berg* formula (equation (1.4)) which derives from the application of the relationship between atomic Einstein A and B coefficients for absorption and spontaneous emission to molecules.

$$k_{\mathrm{r}} = k_0 n^2 = 2.88 \times 10^{-9} n^2 \frac{\int I(\tilde{\nu})\,\mathrm{d}\tilde{\nu}}{\int I(\tilde{\nu})\tilde{\nu}^{-3}\,\mathrm{d}\tilde{\nu}} \int \frac{\varepsilon(\tilde{\nu})}{\tilde{\nu}}\,\mathrm{d}\tilde{\nu}. \tag{4.1}$$

By widefield time-gated fluorescence lifetime imaging, the refractive index of the environment of GFP could be imaged [46], and the lifetime shown to vary approximately as the square of the refractive index. Subsequently, specific GFP-tagged proteins in live cells were studied [47–49] and the initial processes resulting from the encounter of immune system 'natural killer cells' with target cells, where the major histocompatibility complex (MHC) was labelled using GFP showed that the MHC migrates on a short timescale to the synapse between the cells [50,51] (figure 5).

BODIPY fluorescence tags have been shown to have widely differing fluorescence decay times in solvents of varying viscosity (figure 6), fast molecular rotation of one part of the molecule with respect to the other resulting in a competing non-radiative decay of the excited state. This is slowed as the viscosity increases, thus the fluorescence decay time is increased. The effect was exploited in a study of local viscosity in biological cells, reporting on the local viscosity of the immediate environment of the probe [52–59]. This probe technique provides an alternative to directly measured time-resolved fluorescence anisotropy measurements [45]. The probe method may have application in the diagnosis of some diseases, including cancer.

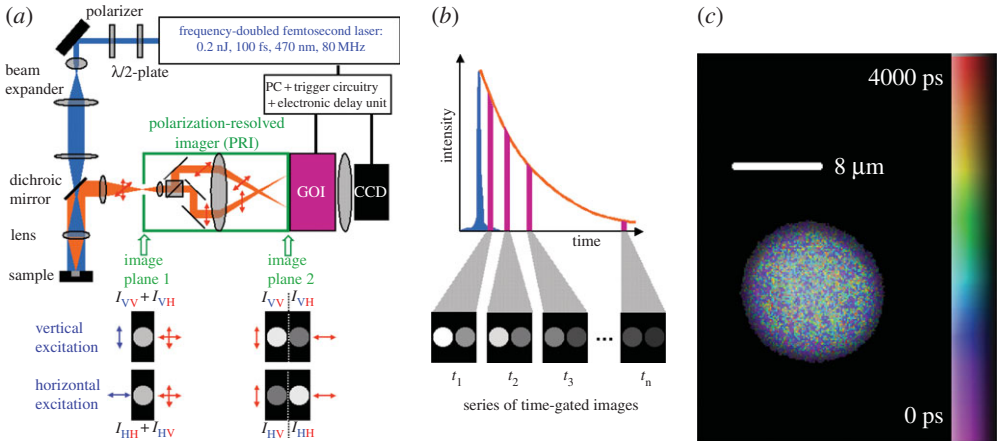

Figure 3. Apparatus for wide-field FLIM and anisotropy measurements [39]. (*a*) Experimental set-up of the wide-field TR-FAIM instrument (polarization-resolved time-gated fluorescence lifetime imaging microscope). The polarization-resolved imager (PRI) contains a polarizing beam-splitter and adjustable mirrors. Using a C-mount adapter, the PRI is mounted on to the gated optical image intensifier (GOI), the output phosphor screen of which is imaged with a CCD camera. The PRI splits a single image in image plane 1 into two spatially identical images differing only in their polarization (image plane 2), which are thus recorded simultaneously. (*b*) A series of such polarization intensity image pairs. (*c*) A rotational correlation time image of a B-cell with stained cytoplasm. (Reproduced from [39] with permission from the European Society for Photobiology, the European Photochemistry Association and the Royal Society of Chemistry). (Online version in colour.)

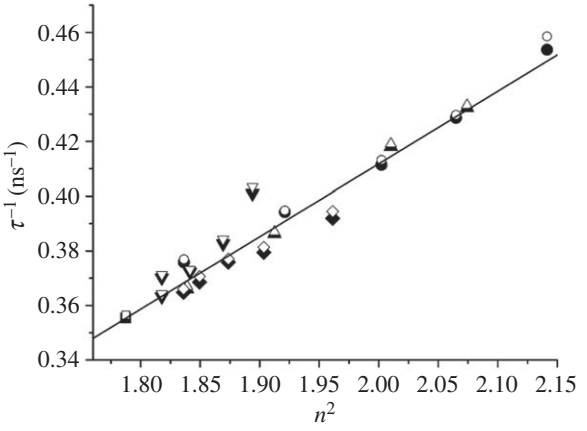

Figure 4. Refractive index dependence of fluorescence decay of green fluorescent protein [46], plot of reciprocal fluorescence decay time against square of refractive index. (Reproduced with permission of Elsevier from [46]).

5. Photodynamic therapy

PDT [60] is the minimally invasive procedure used in treating a range of cancerous diseases, microbial infections and recently, in ophthalmology to treat the wet form of age-related macular degeneration. Photodynamic action has hitherto relied upon the simultaneous interaction between a non-toxic photosensitizer molecule, visible light and molecular oxygen, offering in its most commonly used form, dual selectivity through preferential uptake of the photosensitizer by diseased cells and the selective application of light [61,62]. More recently, forms of light-induced therapy have been developed which do not require oxygen, but we concentrate here on the author's work, where oxygen is a requirement for action.

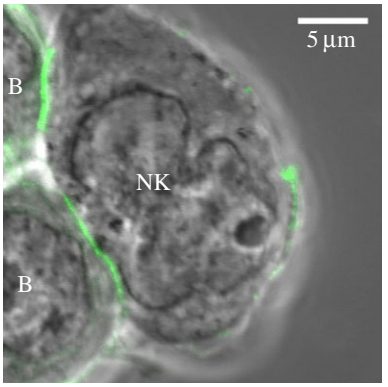

Figure 5. Sequestering of GFP-labelled MHC at the immune synapse GFP fluorescence shows at the contact points of the Natural Killer Cell and the test cells. (D. D. Davis, private communication; see also figure 3*b* in [49]).

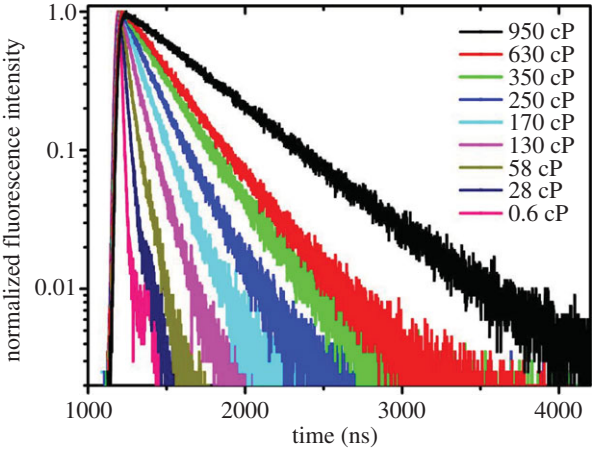

Figure 6. Fluorescence decays of BODIPY molecular rotor dyes in media of differing viscosity [52]. The fluorescence lifetime clearly decreases as the viscosity decreases. (Adapted from figure 1*b*, in [52]).

Following activation with visible light of the appropriate wavelength, the photo sensitizer generates reactive oxygen species (ROS), primarily the reactive singlet state of molecular oxygen, 'singlet oxygen', $O_2(a^1\Delta_g)$, through energy transfer from the long-lived triplet state of the sensitizer to ground state triplet oxygen, $O_2(X^3\Sigma_g^-)$ via an electron exchange mechanism (figure 7).

Other photochemical products of energy and/or electron transfer can include radicals, e.g. the superoxide anion $O_2^{-\bullet}$ and the hydroxyl radical OH•. Production of these reactive species within biological tissues leads to localized cell death via irreversible damage to cellular components such as proteins, lipids and DNA. It should be noted that although singlet oxygen is widely accepted as the dominant mechanism in PDT, electron-transfer processes can, in principle, play a role. Thus, difficult diffuse reflectance studies on the effect of *di-sulfonated aluminium phthalocyanine* photosensitizers on various bacteria (*Streptococcus mutans*, *Porphyromonas gingivalis* and *Escherichia coli*, and the fungus *Candida albicans*) revealed the spectral signature of the radical anion of the sensitizers, clearly implicating electron transfer [63].

The lifetime of singlet oxygen in an aqueous environment is 3.5 µs, which is expected to shorten further in a cellular environment owing to quenching of the singlet oxygen by substrate

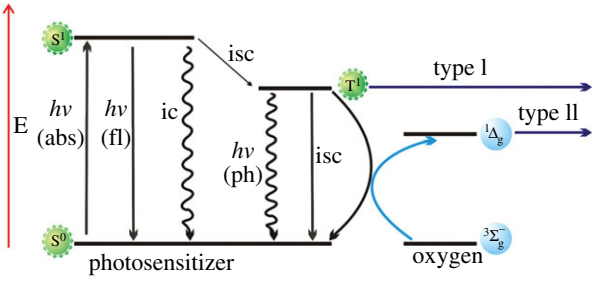

Figure 7. Mechanism of production reactive oxygen species type I leads to radicals, radical ions, etc. through electron transfer; type II to singlet oxygen, presumed to be the major species responsible for cell death in PDT [60,61] by electronic energy transfer from the triplet state. (Reproduced with permission from [62], and reproduced as figure 2 in [61]). (Online version in colour.)

species. (If this were not so, the singlet oxygen would be chemically inert). Spectroscopic data from cells clearly indicate that singlet oxygen is unable to diffuse beyond the intracellular domain where it was produced, in part, owing to a high viscosity of the intracellular environment. Thus, the primary site of ROS generation determines the first point of damage to the cell. Consequently, the subcellular localization as well as the selective accumulation of photosensitizers in diseased cells are important factors in determining PDT efficacy. Fluorescence imaging and FLIM [64–70] have proved to be crucial tools in determining the location of sensitizers in tissue, FLIM and fluorescence decay time measurements [71,72] also providing invaluable information on the intracellular behaviour of these sensitizers.

Tumour destruction post-PDT treatment takes place in two ways, by initiation of necrosis or apoptosis (programmed cell death). Necrosis is caused by sudden cell damage, which leads to the rupture of or damage to the plasma membrane, cell lysis and tissue inflammation. The apoptotic process is initiated when a cell given the appropriate signals begins to shrink. Eventually, the cell is taken up by phagocytes. A tumour may also be destroyed by an indirect process resulting from damage to vasculature associated with the tumour, which is thus starved of nutrients and oxygen, leading to tumour infarction. Tumour hypoxia is both welcomed in PDT, because it leads to ischaemia-related cell death, but has an adverse effect, at the same time, because oxygen is required for the initial PDT process. Most treatments overcome this problem by using fractionated (multiple) light doses with a time interval in between, such that hypoxic tissue is re-oxygenated before the next dose of light.

We have contributed to the PDT field by the provision of novel *phthalocyanine* [73], *porphyrin* [74,75] and *pyropheophorbide–a* [76] photosensitizers; the study of the intracellular distribution of sensitizers in tissue, and the environment of such sensitizers using time-domain fluorescence and diffuse–reflectance flash photolysis methods (see above). In a recent report, Kuimova *et al.* [77] used a *porphyrazine* as both a sensitizer and viscosity marker in cells undergoing PDT. Aggregation is a problem with many if not most sensitizers based upon *porphyrin* and *porphyrin-like* compounds such as *phthalocyanines* and *porphyrazines*. Dimers of most molecules are photochemically inert [but see later section on two-photon excitation (TPE)]' owing to self-quenching of the singlet excited state of these, thus preventing formation of the photochemically active triplet state. A typical case in point is *disulfonated aluminium phthalocyanine* [78] and the corresponding zinc compounds, where the fluorescence and triplet-state yields of these compounds, and the yield of singlet oxygen production are strongly pH-dependent, owing to the formation of inert aggregates at low pH. Unfortunately, the pK_a value for these compounds means that at physiological pH, aggregation still occurs, rendering the sensitizers less than optimal, though still used. *Tri-sulfonated aluminium phthalocyanines* are less aggregated, being more water-soluble, and are used in PDT as 'photosens'. The presence of inert dimers of *aluminium phthalocyanines*, which are capable of quenching dynamically the excited singlet state of the monomeric, active sensitizer is a process that has to be invoked in order to explain

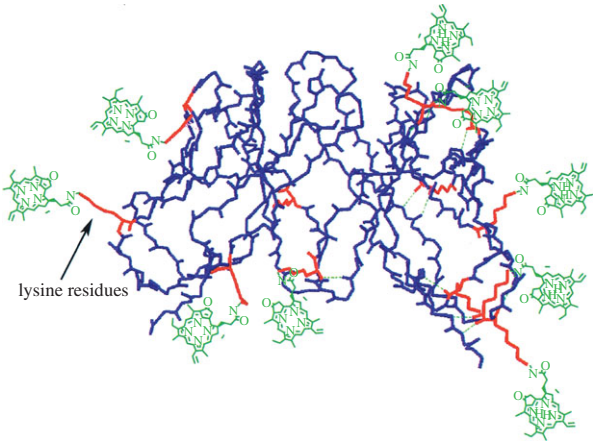

Figure 8. Monoclonal antibody fragment (MAF) sensitizer conjugates [61] Diagrammatic representation of the C6.5 MAF, to which PPa photosensitizers have been covalently linked via the lysine residues on the MAF (Reproduced with permission from [62] and reproduced as figure 8 in [61]).

the photophysics of these compounds in cells [71,72], in lipids and in concentrated aqueous solution [72].

Currently used free sensitizers achieve targeting only in the ratio of 2–5 : 1 tumour to normal tissue; improving this by at least an order of magnitude could reduce dramatically the dosage required for the PDT effect, and reduce considerably side effects such as skin sensitivity.

The principal means to achieve targeting [60,61] include

(i) whole antibodies,
(ii) monoclonal antibody fragments (MAFs),
(iii) peptides, sugars, folic acid,
(iv) multifunctional nanoparticles; and
(v) spatial targeting using TPE.

Whole antibodies have proved to be largely unsuccessful for PDT, owing to solubility problems. Our own work through the company PhotoBiotics, now a subsidiary of Antikor, has concentrated upon single-chain MAFs on which typically 8–10 sensitizers per monoclonal can be achieved [61,79], without causing the aggregation that plagues free sensitizers [71]. The sensitizers are attached to the MAFs via a peptide linkage to the lysine amino acids in the MAF. For some antibodies, lysines in the binding pocket have to be genetically altered so as to prevent attachment of sensitizers in this location, which would eliminate specific binding. The details of the chemistry associated with the attachment of the sensitizer to the MAFs, the choice of targets and comparison with existing sensitizers are all outside the scope of this article. A typical MAF with 10 covalently bound *pheophorbide-a* sensitizers is shown in figure 8, and the enhanced effectiveness of the targeted sensitizer in comparison with the free sensitizer shown in figure 9 in which a thrice-repeated light treatment on mice bearing a human carcinoma is shown to be completely successful in the case of the monoclonal antibody-sensitizer conjugate in eradicating the tumour, whereas the free sensitizer merely arrests growth for a time before re-growth occurs.

The second approach to targeting is that of TPE, such that it is only at the focal point of a pulsed laser that there is sufficient intensity for the two-photon process to occur. The effects are thus spatially confined and thus are controlled by the focusing of the laser. The sensitizers developed by Harry Anderson's group in Oxford have very high cross sections for two-photon absorption, [74,75] and although the one-photon effect for these is poorer in comparison with the commercial sensitizer *Visudyne*, in TPE the *porphyin dimers* are much more effective than *Visudyne*. TPE has the

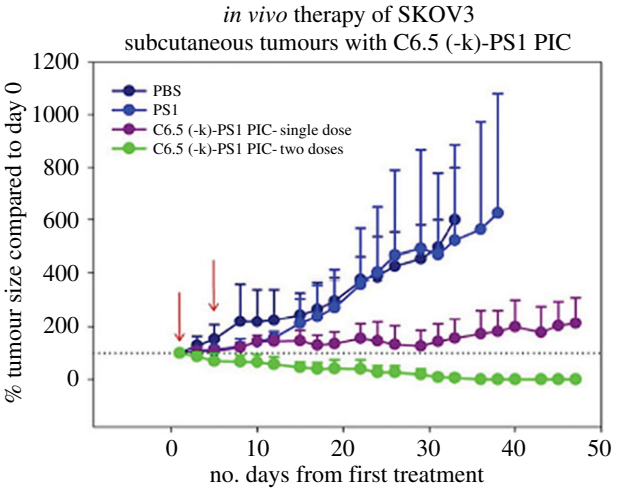

Figure 9. Use of antibody fragment-targeted photosensitizers for PDT [61]. The effect of a free PS1 (see reference [61]), and the same sensitizer attached to the C6.5 MAF on PDT of SKOV cells (see text) compared with no sensitizer (PBS). Clearly, the effect of a double dose of light in the presence of the MAF causes complete eradication of the tumour. (Reproduced with permission from [62], and reproduced as figure 9 in [61]).

advantage of using red or infrared light, which penetrates tissue much more readily that visible light needed for one-photon excitation. The two-photon process may thus have some potential as a means of achieving spatial selectivity in PDT, though it must be admitted that there are practical difficulties associated with focusing lasers within highly scattering media such as human tissue. Nevertheless, the principle has been demonstrated by the two-photon PDT sealing of blood vessels in mice [80].

6. Time-resolved vibrational spectroscopy

Laser development produced ultimately picosecond then subpicosecond pulses of high and reliable intensity, such that detection methods other than fluorescence could be adopted, and time-resolved vibrational spectroscopic (TRVS) techniques came into use, which had the advantage of permitting not only measurement of excited state decay dynamics, but most crucially, gave structural information on the excited states and intermediates in photochemical reactions.

Earliest work involved the measurement of time-resolved resonance Raman spectra of transients on the nanosecond timescale [81–83]; subsequently, this was extended to picosecond resonance Raman [84–86] and then the development of an instrument (PIRATE) at the Rutherford Appleton Laboratories, Oxford, on which picosecond Raman, infrared and transient absorption measurements could be made [87] (figure 10).

More recently, the PIRATE instrument was upgraded to have better time and spectral resolution (ULTRA) [88]. The vision of co-workers at LSF/RAL, notably Tony Parker, Mike Towrie and Pavel Matousek, and co-workers in other universities in particular Ron Hester, York and Mike George, Nottingham should be acknowledged and applauded.

As an example of the use of ultrafast vibrational spectroscopy, some work on charge-transfer excited states will be cited. ICT has often been studied using the molecule 4-DMABN (figure 11) as a model. In non-polar solvents, a single fluorescence band is observed from a locally excited (LE) state of DMABN, whereas in polar solvents, the initially populated LE state reacts further to produce a stable ICT state, which gives rise to a second fluorescence band that overlaps with, but is red-shifted from, the LE emission. While the structures of the LE and ICT states are still disputed

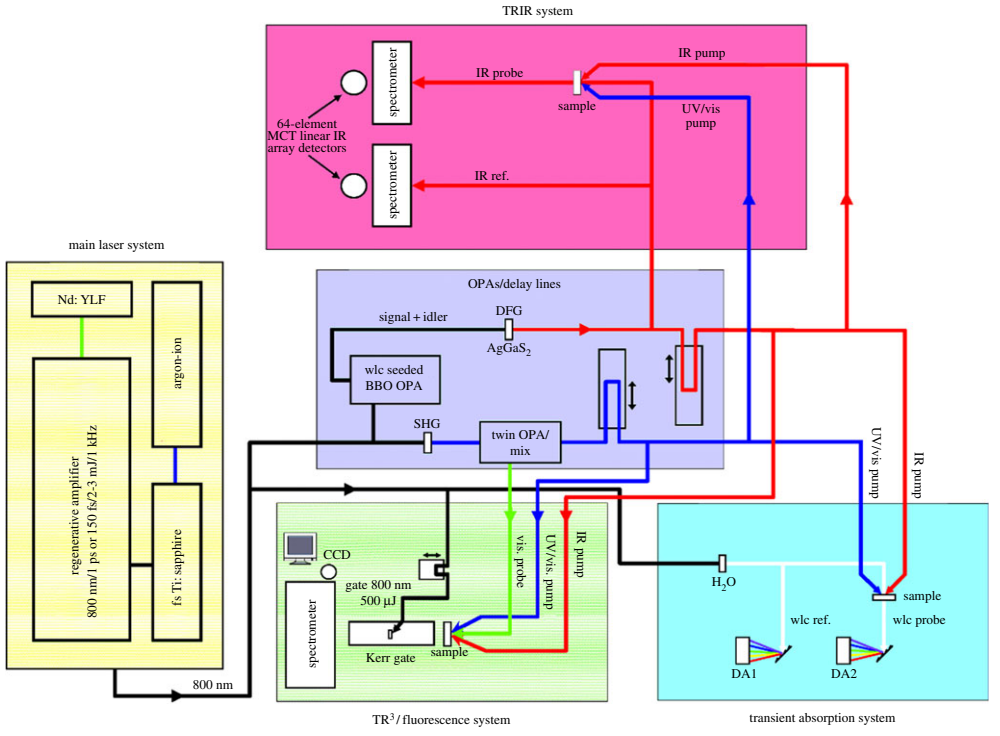

Figure 10. PIRATE ultrafast TRVS system [87]. Schematic layout of the ultrafast time-resolved spectroscopy apparatus (PIRATE) shows how the laser pulses are integrated into the different spectroscopic techniques. (Reproduced with permission from [87]). (Online version in colour.)

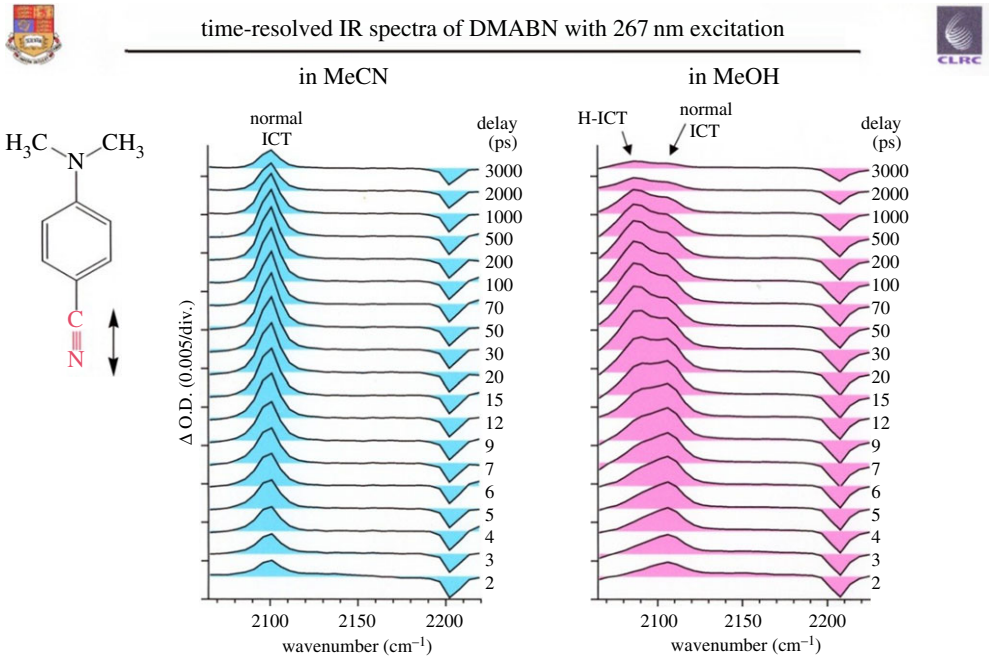

Figure 11. Time-resolved infrared spectra of DMABN in methyl cyanide and methanol solvents [89,90]. The development of two bands corresponding to the cyano group vibration in methanol is seen clearly (see text). (Based on figure 1 in [90].) (Online version in colour.)

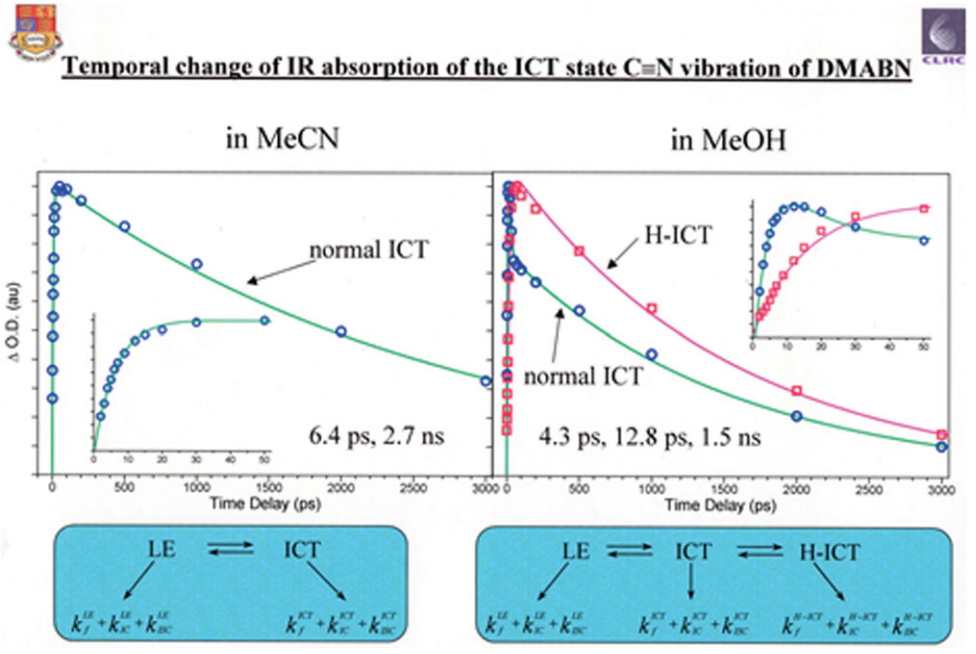

Figure 12. Kinetics of formation and decay of DMABN [87]. (Adapted from figures 2*a*,*b* [90]).

[89,91–93], the difference between the properties of the excited state in protic and aprotic solvents is of interest and is amenable to study by time-resolved infrared (TRIR) measurements [89,90]. For DMABN in the protic solvent methanol (MeOH), the carbon–nitrogen triple bond IR absorption band develops from an initial single band into a doublet. The initial single band was interpreted as belonging to an ICT state like that created in aprotic acetonitrile (MeCN), where only one absorption band is observed at all delay times. The second component was interpreted as being due to a hydrogen-bonded charge transfer state, designated HICT. Figure 11 shows TRIR spectra of DMABN in MeCN (*a*) and MeOH (*b*) recorded with subpicosecond time resolution at pump–probe delays from 2 to 3000 ps after excitation; the kinetics in figure 12 give the time-dependence of the absorption band areas, and show the populations of the free and hydrogen-bonded species coming to dynamic equilibrium. This was the first *direct* observation of hydrogen bonding in an excited state.

In more detail, time constants for the non-radiative reaction LE to ICT plus the decay of the whole population (lines in figure 12*a*) are 6.4 ps (equilibration) and 2.7 ns decay. The results obtained are very different in MeOH (figure 12*b*). As the carbon nitrogen triple bond band absorption grows, it can be resolved into two components at 2091 and 2109 cm^{-1}, which reach constant relative intensities by about 50 ps. Ground-state bleach recovery can be seen in figure 12*b*, and the enhancement relative to the behaviour in MeCN indicates much stronger internal conversion in MeOH. Qualitatively similar results were obtained in ethanol and butanol. The growth of the component at 2091 cm^{-1} at the expense of that at 2109 cm^{-1} is clearly due to an interaction that occurs in protic MeOH after charge separation and does not occur in aprotic MeCN. As stated earlier, we attribute it to hydrogen bonding between the MeOH and the ICT state of DMABN. The kinetics are well described (lines in figure 12*b*) by a sequence of reversible, non-radiative reactions that lead to equilibrium populations on picosecond timescales with each excited state also decaying on the nanosecond timescale as discussed earlier. Intermolecular solute–solvent hydrogen bonding interactions are highly sensitive to solute–solvent orientation and distance, and the formation process must also compete with the tendency of MeOH to form solvent–solvent multimers. It is therefore significant that the estimated time constant for the

forward hydrogen-bonding reaction is close to the 15.8 ps timescale for solvent–solvent bond breaking and C–OH rotation in MeOH. The charge-separation step is thus seen to be necessary to favour DMABN–MeOH configurations that form bonds having lifetimes of a few picoseconds, so that the majority of the DMABN excited-state population becomes hydrogen bonded, despite the strong MeOH–MeOH interaction. The overall fluorescence spectrum must thus be composed of contributions from LE, ICT and HICT. We have proposed that this novel three-state mechanism can account for many anomalies in the fluorescence spectra of dual fluorescence molecules in protic solvents. The results also illustrate the power of the high-resolution, high-sensitivity TRIR technique employed and the ability to monitor the formation of bonds between excited states in real time.

A further example of the use of TRVS in the field of organometallic compounds by one of the pioneers of PIRATE and ULTRA is also cited here [94].

7. Summary

We have traced the development of ultrafast fluorescence and time-resolved vibrational spectroscopies throughout the career of the author, from nanosecond to subpicosecond. The uses of these techniques by the author and his successive research groups to study the decay of molecular systems have been described, with particular emphasis on fluorescence lifetime imaging microscopy, the use of this technique in the treatment of cancer and bacterial infections through PDT, and in other biological systems. The apparatus developed in Rutherford Appleton Laboratories for time-resolved vibrational spectroscopies, initially resonance Raman on the nanosecond timescale, through to Raman and TRIR on the picosecond timescale is illustrated with reference to studies on DMABN a prototypical molecule displaying ICT.

Competing interests. I declare we have no competing interests.

Funding. I received no funding for this study.

Acknowledgements. It is a pleasure to acknowledge my gratitude to the some 60 PhD students, 50 master's degree students, 50+ post-doctoral fellows and numerable academic visitors whom I have had the enormous benefit of working with over my career. My co-workers in the University of Southampton, the Royal Institution of Great Britain, Imperial College London and LSF at Rutherford Appleton Laboratories have also contributed to the very great pleasure I have enjoyed in photochemistry research. Financial support, gratefully received over the years, has come from The Royal Society, SERC, EPSRC, US Army European Research Office, NATO, The Waldburg Trust, Unilever, Monsanto and others.

References

1. O'Connor DV, Phillips D. 1984 *Time-correlated single photon counting*. London, UK: Academic Press.
2. Becker W, Hickl B. 2015 *The bh TCSPC handbook*, 6th edn. Becker & Hickl GmbH, www.becker-hickl.com.
3. Rumbles G, Phillips D. 1882 Iterative reconvolution techniques used in the analysis of fluorescence decay curves in terms of multiple components. In *'Convolution–reconvolution'* (ed. M Bouchy), pp. 425–444.
4. Ghiggino KP, Roberts AJ, Phillips D. 1980 Time-resolved fluorescence spectroscopy using pulsed lasers. *J. Phys. E* **13**, 446–450. (doi:10.1088/0022-3735/13/4/019)
5. Beddard GS, Doust T, Meech SR, Phillips D. 1981 Synchronously-pumped dye laser in fluorescence decay measurements of molecular motion. *J. Photochem.* **17**, 427–433. (doi:10.1016/0047-2670(81)85386-5)
6. Roberts AJ, Phillips D. 1983 Time-resolved fluorescence spectroscopy using pulsed laser. In *Quantum electronics and electro-optics* (ed. PL Knight), pp. 143–144. London, UK: Wiley.
7. Doust T, Porter G, Phillips D. 1984 Picosecond spectroscopy: applications in biochemistry. Part I: techniques. *Biochem. Soc. Trans.* **12**, 628–630. (doi:10.1042/bst0120630)
8. Doust T, Porter G, Phillips D. 1984 Picosecond spectroscopy: applications in biochemistry. Part II: applications. *Biochem. Soc. Trans.* **12**, 633–635. (doi:10.1042/bst0120633)

9. Phillips D, Drake RC, O'Connor DV, Christensen RL. 1985 Time-correlated single-photon counting using laser excitation. *Anal. Instrum.* **14**, 267–292. (doi:10.1080/10739148508543581)
10. O'Connor DV, Roberts AJ, Phillips D. 1981 On the construction of nanosecond time-resolved emission spectra. *Photochem. Photobiol.* **33**, 159–172. (doi:10.1111/j.1751-1097.1981.tb05319.x)
11. O'Connor DV, Roberts AJ, Lampert RA, Meech SR, Chewter L, Phillips D. 1983 Standards for nanosecond fluorescence decay time measurements. *Anal. Chem.* **55**, 68–73. (doi:10.1021/ac00252a020)
12. Meech SR, Phillips D. 1983 Photophysics of some common fluorescence standards. *J. Photochem.* **23**, 193–217. (doi:10.1016/0047-2670(83)80061-6)
13. Boens N *et al*. 2007 Fluorescence lifetime standards for time and frequency domain fluorescence spectroscopy. *Anal. Chem.* **79**, 2137–2149. (doi:10.1021/ac062160k)
14. Ghiggino KP, Roberts AJ, Phillips D. 1978 Energy relaxation in synthetic polymer solutions. *J. Photochem.* **9**, 301–303. (doi:10.1016/0047-2670(78)80152-X)
15. Phillips D, Roberts A, Soutar I. 1980 Transient decay studies of photophysical processes in aromatic polymers. I. Fluorescence decays in copolymers of 1-vinyl naphthalene and methacrylate. *J. Polym. Sci. Polym. Phys.* **18**, 2401–2413. (doi:10.1002/pol.1980.180181208)
16. Roberts AJ, O'Connor DV, Phillips D. 1981 Multicomponent fluorescence decay in vinyl aromatic polymers and copolymers. *Ann. N.Y. Acad. Sci.* **366**, 109–124. (doi:10.1111/j.1749-6632.1981.tb20749.x)
17. Carey MJ, Phillips D. 1994 Modelling excimer formation in vinyl aromatic polymers. *Chem. Phys.* **185**, 75–89. (doi:10.1016/0301-0104(94)00102-2)
18. Soutar I, Swanson L, Christensen RL, Drake RC, Phillips D. 1996 Time-resolved luminescence anisotropy studies of the relaxation behaviour of polymers: 1. Intramolecular segmental relaxation of poly(methylmethacrylate) and poly-(methylacrylate) in dilute solutions in dichloromethane. *Macromolecules* **29**, 4931–4936. (doi:10.1021/ma951671y)
19. Carey MJ, Phillips D. 2000 Fluorescence kinetics of co-polymers of 1-vinylnaphthalene and methyl methacrylate. *Eur. Polym. J.* **36**, 619–624. (doi:10.1016/S0014-3057(99)00106-8)
20. Brown AJ, Rumbles G, Phillips D. 1991 Time-resolved evanescent wave-induced fluorescence spectroscopy I deviations in silica/methanol interface. *JCS Faraday Trans.* **87**, 825–830. (doi:10.1039/FT9918700825)
21. Rumbles G, Brown AJ, Phillips D. 1992 Surface-induced chromism and enhanced fluorescence of the soluble poly(diacetylene) poly 4 BCMU at a solid/solution interface; an evanescent wave-induced fluorescence study. *JCS Faraday Trans.* **88**, 3313–3318. (doi:10.1039/ft9928803313)
22. Rumbles G, Bloor D, Brown AJ, de Mello AJ, Crystall B, Phillips D, Smith TA. 1994 Time-resolved evanescent wave-induced fluorescence studies of polymer-surface interactions. In *Spectroscopy and chemistry in small domains* (ed. H Masuhara), pp. 269–286. Amsterdam, The Netherlands: Elsevier Science Publishers.
23. Ghiggino KP, Lee AG, Meech SR, O'Connor DV, Phillips D. 1981 Time-resolved emission spectroscopy of the dansyl fluorescence probe. *Biochemistry* **20**, 5381–5389. (doi:10.1021/bi00522a005)
24. Meech SR, Phillips D, Lee AG. 1982 Time-resolved emission spectroscopy of 1,3 dimethyl indole in *n*-butanol. *Chem. Phys. Lett.* **92**, 523–527. (doi:10.1016/0009-2614(82)87053-X)
25. Meech SR, Phillips D, Lee AG. 1983 On the nature of the fluorescent state of methylated indole derivatives. *Chem. Phys.* **80**, 317–328. (doi:10.1016/0301-0104(83)85286-0)
26. Meech SR, Stubbs CD, Phillips D. 1984 The application of fluorescence decay measurements in studies of biological systems. *IEE J. Quantum Electron.* **20**, 1343–1352. (doi:10.1109/JQE.1984.1072320)
27. Bayley PM, Beeby A, Janot J-M, Phillips D. 1991 The time-resolved fluorescence and anisotropy of subtilisins BPN' and Carlsberg. *Biophys. Chem.* **41**, 277–282. (doi:10.1016/0301-4622(91)85042-O)
28. Meech SR, O'Connor DV, Phillips D. 1983 The photophysics of 1-aminonaphthalenes. *JCS (Faraday Trans. II)*. **79**, 1563–1584. (doi:10.1039/f29837901563)
29. O'Connor DV, Meech SR, Phillips D. 1982 Complex fluorescence decay of quinine bisulphate in aqueous sulphuric acid solution. *Chem. Phys. Lett.* **88**, 22–26. (doi:10.1016/0009-2614(82)80062-6)
30. Meech SR, Phillips D. 1987 Time-resolved fluorescence of p-dimethylaminobenzonitrile in mixed solvents. *J. C. S. Faraday II* **83**, 191–195. (doi:10.1039/f29878301941)

31. Auty AR, Jones AC, Phillips D. 1984 Fluorescence excitation spectra and decay times of jet-cooled dibenzofuran and dibenzofuran-water complex. *Chem. Phys. Lett.* **112**, 529–533. (doi:10.1016/0009-2614(84)85771-1)
32. Ichimura T, Auty AR, Jones AC, Phillips D. 1985 The fluorescence lifetimes of jet-cooled alkylnaphthalenes. *Bull. Chem. Soc. Japan* **58**, 2407–2408. (doi:10.1246/bcsj.58.2407)
33. Jones AC, Auty AR, Phillips D. 1986 Spectroscopy and decay dynamics of jet-cooled carbazole and N-ethyl carbazole and their homocyclic analogues. *Chem. Phys.* **103**, 163–182. (doi:10.1016/0301-0104(86)85111-4)
34. Scully AD, MacRobert AJ, Botchway S, O'Neill P, Parker AW, Ostler RB, Phillips D. 1996 Development of a laser-based fluorescence microscope with sub-nanosecond time resolution. *J. Fluorescence* **6**, 119–125. (doi:10.1007/BF00732051)
35. Eigenbrot IV, Crystall B, Phillips D. 1996 A versatile time-resolved laser scanning confocal microscope. In *Fluorescence microscopy and fluorescent probes* (ed. J Slavik), pp. 86–92. New York, NY: Plenum Press.
36. Hirayama S, Phillips D. 1980 Correction for refractive index in the comparison of radiative lifetimes in vapour and solution phases. *J. Photochem.* **12**, 139–146. (doi:10.1016/0047-2670(80)85036-2)
37. Lampert RA, Meech SR, Metcalfe J, Phillips D, Schaap AP. 1983 The refractive index correction to the radiative rate constant in fluorescence lifetime measurements. *Chem. Phys. Lett.* **94**, 137–140. (doi:10.1016/0009-2614(83)87560-5)
38. Webb SED *et al*. 2005 A wide-field time-domain fluorescence lifetime imaging microscope with optical sectioning. *Rev. Sci. Instrum.* **73**, 1898–1907. (doi:10.1063/1.1458061)
39. Suhling K, French PMW, Phillips D. 2005 Time-resolved fluorescence microscopy. *Photochem. Photobiol. Sci.* **4**, 13–22. (doi:10.1039/b412924p)
40. Dowling K, Hyde SCW, Dainty JC, French PMW, Hares JD. 1997 2-D fluorescence lifetime imaging using a time-gated image intensifier. *Opt. Commun.* **135**, 27–31. (doi:10.1016/S0030-4018(96)00618-9)
41. Becker W, Bergmann A, Hink MA, Konig K, Benndorf K, Biskup C. 2004 Fluorescence lifetime imaging by time-correlated single-photon counting. *Microsc. Res. Tech.* **63**, 58–66. (doi:10.1002/jemt.10421)
42. Krishnan RV, Biener E, Zhang JH, Heckel R, Herman B. 2003 Probing subtle fluorescence dynamics in cellular proteins by streak camera based fluorescence lifetime imaging microscopy. *Appl. Phys. Lett.* **83**, 4658–4660. (doi:10.1063/1.1630154)
43. Lakowicz JR, Berndt K. 1991 Lifetime-selective fluorescence imaging using an RF phase-sensitive camera. *Rev. Sci. Instrum.* **62**, 1727–1734. (doi:10.1063/1.1142413)
44. Carlsson K, Liljeborg A. 1998 Simultaneous confocal lifetime imaging of multiple fluorophores using the intensity-modulated multiple-wavelength scanning (IMS) technique. *J. Microsc.* **191**, 119–127. (doi:10.1046/j.1365-2818.1998.00362.x)
45. Siegel J, Suhling K, Leveque-Fort S, Webb SED, Davis DM, Phillips D, Sabharwal Y, French PMW. 2003 Wide-field time-resolved fluorescence anisotropy imaging (TR-FAIM): imaging the rotational mobility of a fluorophore. *Rev. Sci. Instrum.* **74**, 182–192. (doi:10.1063/1.1519934)
46. Suhling K, Siegel J, Phillips D, French PWM, Leveque-Fort S, Webb SED, Davis DM. 2002 Imaging the environment of green fluorescent protein, GFP. *Biophys J.* **83**, 3589–3595. (doi:10.1016/S0006-3495(02)75359-9)
47. Suhling K, Siegel J, Lanigan PMP, Leveque-Fort S, Webb SED, Phillips D, Davis DM, French PMW. 2004 Time-resolved fluorescence anisotropy imaging applied to live cells. *Opt. Lett.* **29**, 584–586. (doi:10.1364/OL.29.000584)
48. Suhling K, Davis DM, Phillips D. 2002 The influence of solvent viscosity on the fluorescence decay and time-resolved anisotropy of green fluorescent protein GFP. *J. Fluorescence* **12**, 91–95. (doi:10.1023/A:1015323606154)
49. Elson DS *et al*. 2004 Time-domain fluorescence lifetime imaging applied to biological tissue. *Photochem. Photobiol. Sci.* **3**, 795–801. (doi:10.1039/b316456j)
50. Treanor B, Lanigan PMP, Suhling K, Schreiber T, Munro I, Neil MAA, Phillips D, Davis DM, French PMW. 2005 Imaging fluorescence lifetime heterogeneity applied to GFP-tagged MHC protein at an immunological synapse. *J. Microsc.* **217**, 36–43. (doi:10.1111/j.0022-2720.2005.01430.x)

51. Treanor B *et al*. 2006 Microclusters of inhibitory killer immunoglobulin-like receptor signaling at natural killer cell immunological synapses. *J. Cell Biol.* **174**, 153–161. (doi:10.1083/jcb.200601108)
52. Levitt JA, Kuimova MK, Yahioglu G, Chung P-H, Suhling K, Phillips D. 2008 Membrane-bound molecular rotors measure viscosity in live cells via fluorescence lifetime imaging. *J. Phys. Chem. C* **113**, 11 634–11 642. (doi:10.1021/jp9013493)
53. Hosny NK *et al*. 2013 Mapping microbubble viscosity using fluorescence lifetime imaging of molecular rotors. *Proc. Natl Acad. Sci. USA* **110**, 9225–9230. (doi:10.1073/pnas.1301479110)
54. Wu Y *et al*. 2013 Molecular rheometry: direct determination of viscosity in Lo and Ld lipid phases via fluorescence lifetime imaging. *Phys. Chem. Chem. Phys.* **15**, 14 986–14 993. (doi:10.1039/c3cp51953h)
55. Loison P, Hosny NA, Gervais P, Champion D, Kuimova MK, Perrier-Cornet J-M. 2013 Direct investigation of viscosity of an atypical inner membrane of *Bacillus* spores: a molecular rotor/FLIM study. *Biochim. Biophys. Acta Biomembr.* **1828**, 2436–2443. (doi:10.1016/j.bbamem.2013.06.028)
56. Lopez-Duarte I, Vu TT, Izquierdo MA, Bull JA, Kuimova MK. 2014 A molecular rotor for measuring viscosity in plasma membranes of live cells. *Chem. Commun.* **50**, 5282–5284. (doi:10.1039/C3CC47530A)
57. Thompson J, Herling T, Kubánková M, Vyšniauskas A, Knowles T, Kuimova MK. 2015 Molecular rotors provide insights into microscopic structural changes during protein aggregation. *J. Phys. Chem. B* (doi:10.1021/acs.jpcb.5b05099)
58. Vyšniauskas A, Qurashi M, Gallop N, Balaz M, Anderson HL, Kuimova MK. 2015 Unravelling the effect of temperature on viscosity-sensitive fluorescent molecular rotors. *Chem. Sci.* (doi:10.1039/C5SC02248G)
59. Dent MR *et al*. 2015 Imaging phase separation in model lipid membranes through the use of BODIPY based molecular rotors. *Phys. Chem. Chem. Phys.* **17**, 18 393–18 402. (doi:10.1039/C5CP01937K)
60. Kuimova MK, Phillips D. 2013 *Photomedicine*. In *Applied photochemistry* (eds. RC Evans, P Douglas, HD Burrow). Dordrecht, NY: Springer.
61. Phillips D. 2011 Towards targeted photodynamic therapy. *Pure Appl. Chem.* **83**, 733–748. (doi:10.1351/PAC-CON-11-01-05)
62. Stamati I. 2010 Targeted PDT for cancer using photoimmunoconjugates based on pyropheophorbide-a derivatives. PhD Thesis, Imperial College, London.
63. Oldham TC, Phillips D. 1999 Flash photolysis of sensitzers in microbes. *J. Phys. Chem.* **103**, 9333–9349. (doi:10.1021/jp991438s)
64. Petrasek Z, Ostler RB, Eigenbrot IV, Phillips D. 1999 Fluorescence decay kinetics and localisation of disulphonated aluminium phthalocyanine in fibroblasts – a confocal fluorescence microscopy study. *SPIE Proc.* **3602**, 285–297. (doi:10.1117/12.347547)
65. Ambroz M, MacRobert AJ, Morgan J, Rumbles G, Foley MSC, Phillips D. 1994 Time-resolved fluorescence spectroscopy and intracellular imaging of disulphonated aluminium phthalocyanine. *J. Photochem. Photobiol. B.* **22**, 105–117. (doi:10.1016/1011-1344(93)06955-3)
66. Scully AD, Ostler RB, MacRobert AJ, Parker AW, de Lara C, O'Neil P, Phillips D. 1998 Laser line-scanning confocal fluorescence imaging of the photodynamic ac of aluminium and zinc phthalocyanines in V7904 Chinese hamster fibroblasts. *Photochem. Photobiol.* **68**, 199–204.
67. Scully AD, Ostler RB, Phillips D, O'Neill P, Townsend KMS, Parker AW, MacRobert AJ. 1997 Application of fluorescence lifetime imaging microscopy, to the investigation of intracellular PDT mechanisms. *Bioimaging* **5**, 9–18. (doi:10.1002/1361-6374(199703)5:1<9::AID-BIO2>3.3.CO;2-1)
68. Connelly JP, Botchway SW, Kunz L, Pattison D, Parker AW, MacRobert AJ. 2001 Time-resolved fluorescence imaging of photosensitiser distributions in mammalian cells using a picosecond laser line-scanning microscope. *J. Photochem. Photobiol. A Chem.* **142**, 169–175. (doi:10.1016/S1010-6030(01)00511-1)
69. Ruck AC, Kress M, Dolp F, Akgun N, Meier T, Steiner R. 2002 New Microscopic techniques to investigate intracellularlocalization and reactions of photosensitizers. Laser scanning fluorescence lifetime imaging (LS-FLIM). *Med. Laser Appl.* 41–47. (doi:10.1078/1615-1615-00045)
70. Kress M, Meier T, Steiner R, Dolp F, Erdmann R, Ortmann U, Ruck A. 2003 Time-resolved microspectrofluorometry and fluorescence lifetime imaging of photosensitizers

using picosecond pulse diode lasers in laser scanning microscopes. *J. Biomed. Opt.* **8**, 26–32. (doi:10.1117/1.1528595)
71. Petrasek Z, Phillips D. 2003 A time-resolved study of concentration quenching of disulphonated aluminium phthalocyanine fluorescence. *Photochem. Photobiol. Sci.* **2**, 236–244. (doi:10.1039/B209906C)
72. Lacey JA, Phillips D. 2002 Fluorescence lifetime measurements of disulphonated aluminium phthalocyanine in the presence of microbial cells. *Photochem. Photobiol. Sci.* **1**, 378–383. (doi:10.1039/b108831a)
73. Phillips D. 1997 Chemical mechanisms in photodynamic therapy with phthalocyanines. *Progr. React. Kinet.* **22**, 175–300.
74. Kuimova MK. 2008 Photophysical properties and intracellular imaging of water-soluble porphyrin dimers for two-photon excited photodynamic therapy. *Org. Biomol. Chem.* **7**, 889–896. (doi:10.1039/b814791d)
75. Dahlstedt E, Collins HA, Balaz M, Kuimova MK, Khurana M, Wilson BC, Phillips D, Anderson HL. 2008 One and two-photon activated phototoxicity of conjugated porphyrin dimers with high two-photon absorption cross-sections. *Org. Mol. Biochem.* **7**, 897–904.
76. Stamata I, Kuimova MK, Lion M, Yahioglu G, Phillips D, Deonarain MP. 2010 Novel photosensitisers derived from pyropheophorbide-a:uptake by cells and photodynamic efficiency *in vivo*. *Photchem. Photobiol. Sci* **9**, 1033–1041. (doi:10.1039/c0pp00038h)
77. Izquierdo MA, Vyšniauskas A, Lermontova SA, Grigoryev IS, Shilyagina NY, Balalaeva IV, Klapshina LG, Kuimova MK. 2015 Dual use of porphyrazines as sensitizers and viscosity markers during photodynamic therapy. *J. Mater. Chem. B* **3**, 1089–1096. (doi:10.1039/C4TB01678E)
78. Phillips D, Dhami S, Ostler RB, Petrasek Z. 2003 The dimerisation of phthalocyanines. *Progr. React. Kinet. Mech.* **28**, 299–420. (doi:10.3184/007967403322807390)
79. Kuimova MK, Bhatti M, Deonarain M, Yahioglu G, Levitt JA, Stamati I, Suhling K, Phillips D. 2007 Fluorescence characterisation of multiply-loaded anti-HER2 single chain Fv-photosensitiser conjugates suitable for photodynamic therapy. *Photochem. Photobiol. Sci.* **6**, 933–939. (doi:10.1039/b708320c)
80. Collins HA *et al*. 2008 Blood vessel closure via two-photon excitation of a conjugated porphyrin dimer. *Nat. Photon.* **2**, 420–425. (doi:10.1038/nphoton.2008.100)
81. Moore JN, Atkinson GH, Phillips D, Killough PM, Hester RE. 1984 Time-resolved resonance Raman spectroscopy of the radical anion of disodium anthraquinone-2,6-disulphonate. *Chem. Phys. Lett.* **107**, 381–384. (doi:10.1016/S0009-2614(84)80239-0)
82. Moore JN, Phillips D, Hester RE. 1988 Time-resolved resonance Raman spectroscopy applied to the photochemistry of the sulphonated derivatives of 9,10-anthraquinone. *J. Phys. Chem.* **92**, 5619–5627. (doi:10.1021/j100331a017)
83. Vauthey E, Phillips D. 1990 Viscosity effect on the rate of back-electron transfer within a short-lived exciplex. *Chem. Phys.* **147**, 421–430. (doi:10.1016/0301-0104(90)85056-3)
84. Ma C, Kwok WM, Matousek P, Parker AW, Phillips D, Toner WT, Towrie M. 2001 Resonance Raman study of ring deuterated 4-dimethylaminobenzonitrile (DMABN-d4); the ground, ICT and triplet states. *J. Photochem. Photobiol. A. Chem.* **142**, 177–186. (doi:10.1016/S1010-6030(01)00512-3)
85. Parker AW, Towrie M, Matousek P, Vauthey DPE. 1997 Investigating photo-initiated electron transfer reactions using time-resolved resonance Raman spectroscopy. In *Proc. 7th Int. Conf. on time-resolved vibrational spectroscopy* (ed. B Woodruff). Springer Proceedings in Physics, Springer.
86. Matousek P, Towrie M, Ma C, Kwok WM, Phillips D, Toner WT, Parker AW. 2001 Fluorescence suppression in resonance Raman spectroscopy using a high performance picosecond Kerr gate. *J. Raman Spectrosc.* **32**, 983–988. (doi:10.1002/jrs.784)
87. Towrie M *et al*. 2003 Development of a broadband picosecond time-resolved infrared spectrometer and its incorporation into an existing ultrafast time-resolved resonance Raman, UV/visible and fluorescence spectroscopic apparatus. *Appl. Spectrosc.* **57**, 367–380. (doi:10.1366/00037020360625899)
88. Greetham GM *et al*. 2010 ULTRA - a unique instrument for time-resolved spectroscopy. *Appl. Spectrosc.* **64**, 1311–1319. (doi:10.1366/000370210793561673)
89. Kwok WM, Ma C, George MW, Grills DC, Matousek P, Parker AW, Phillips D, Toner WT, Towrie M. 2007 Solvent effects on the charge-transfer excited states of 4-dimethyl amino

benzonitrile [DMABN] and 4-dimethylamino-3,5-dimethyl aminobenzonitrile [TMABN] studied by time- resolved infra-red spectroscopy: a direct observation of hydrogen-bonding interactions. *Photochem. Photobiol. Sci.* **6**, 987–994. (doi:10.1039/b708414e)

90. Kwok WM, George MW, Grills DC, Ma C, Matousek P, Parker AW, Phillips D, Toner WT, Towrie M. 2003 Direct observation of a hydrogen-bonded charge-transfer state of 4-dimethylaminobenzonitrile, [DMABN] in methanol by time-resolved infra-red spectroscopy. *Angew. Chem. Int. Ed.* **42**, 1826–1830. (doi:10.1002/anie.200219816)
91. Ma C, Kwok WM, Matousek P, Parker AW, Phillips D, Toner WT, Towrie M. 2002 Excited states of 4-aminobenzonitrile [ABN] and 4-dimethylaminobenzonitrile [DMABN]:time-resolved resonance Raman, transient absorption and ab initio calculations. *J. Phys. Chem. A* **106**, 3294–3305. (doi:10.1021/jp012765e)
92. Kwok WM, Ma C, Matousek P, Parker AW, Phillips D, Toner WT, Towrie M, Zuo P, Phillips DL. 2003 Time-resolved spectroscopy study of the triplet state of 4-diethylamino benzonitrile [DEABN]. *PCCP* **5**, 3643–3652. (doi:10.1039/b304896a)
93. Kwok WM, Ma C, George MW, Grills DC, Matousek P, Parker AW, Phillips D, Toner WT, Towrie M. 2003 Further time-resolved spectroscopic investigations in the intramolecular charge -transfer state of 4-dimethyl aminonenzonitrile [DMABN], and its derivatives 4-diethylaminobenzonitrile,[DEABN], and 4-dimethylamino-3,5-dimethylamino benzonitrile [TMABN]'. *PCCP* **5**, 1043–1050. (doi:10.1039/b209621h)
94. Brookes CM, Lomont JP, Nguyen SC, Calladine JA, Sun X-Z, Harris CB, George MW. 2014 New insights into the photochemistry of $[CpFe(CO)_2]2$ using picosecond through microsecond time-resolved infrared spectroscopy (TRIR). *Polyhedron* **72**, 130–134. (doi:10.1016/j.poly.2013.12.028)